An innovative and environmentally friendly bioorganic synthesis of activated carbon based on olive stones and its potential application for

Sustainable Materials and Technologies 38 (2023) e00717

Contents lists available at ScienceDirect

Sustainable Materials and Technologies

journal homepage: www.elsevier.com/locate/susmat

Research Paper

An innovative and environmentally friendly bioorganic synthesis of activated carbon based on olive stones and its potential application for CO_2 capture

Jarosław Serafin [a,*], Bartosz Dziejarski [b,c], Joanna Sreńscek-Nazzal [d]

[a] Department of Inorganic and Organic Chemistry, University of Barcelona, Martí i Franquès, 1-11, 08028 Barcelona, Spain
[b] Faculty of Environmental Engineering, Wroclaw University of Science and Technology, 50-370 Wroclaw, Poland
[c] Department of Space, Earth and Environment, Division of Energy Technology, Chalmers University of Technology, SE-412 96 Gothenburg, Sweden
[d] West Pomeranian University of Technology in Szczecin, Faculty of Chemical Technology and Engineering, Department of Catalytic and Sorbent Materials Engineering, Piastów Ave. 42, 71-065 Szczecin, Poland

ARTICLE INFO

Keywords:
Novel bioorganic synthesis
Activated carbon
Eco-friendly activating agent
Olive stones
CO_2 adsorption
CO_2/N_2 selectivity

ABSTRACT

This work presents an innovative, fully environmentally friendly method of obtaining bioorganic activated carbon based on olive stones by applying banana plant extract as an activating agent. The activated carbon prepared in this way was compared with activated carbons prepared by chemical activation using potassium hydroxide (KOH) and phosphoric acid (H_3PO_4). The obtained results of physicochemical characterization were comparable to the currently commonly obtained activated carbons. For the novel activated carbon, the specific surface area was equal to 915 m^2/g, and the pore area was 0.495 cm^3/g. The CO_2 adsorption capacity of the newly obtained activated carbon was also tested and it was 6.32 mmol/g and 4.33 mmol/g for 0 °C and 30 °C, respectively. This material has a high selectivity equal to 161.1 and stability after the 50th adsorption-desorption cycles. The material prepared in this way creates new possibilities for obtaining high-quality activated carbon and it does away with the requirement for using any hazardous inorganic activating agent like acids or bases, which makes it completely harmless to the environment.

1. Introduction

Global CO_2 emissions are increasing at an alarming rate and have had the highest negative impact among other greenhouse gases on the natural environment for decades, leading to global warming and climate change [1,2]. This trend is expected to continue, as carbon dioxide comes from a variety of sources, including burning fossil fuels in power and combined heat and power plants; deforestation; livestock farming; and facilitating industrialization along with the progress of civilization that severely affects the climate and temperature of the Earth [3]. Considering the above, the reduction of CO_2 emissions has become one of the main goals of highly industrialized nations and private industries worldwide in the sense that it establishes a worldwide framework to prevent severe climate change by keeping global warming at far below 2 °C, as stated in the Paris Agreement. Unfortunately, according to the International Energy Agency (IEA), as a result of a robust recovery from economic stagnation from the worldwide COVID-19 emergency, global energy-related carbon dioxide emissions increased by 6% in 2021, reaching 36.3 billion tonnes [4]. This was the highest level ever recorded in history compared to 2010. Due to these factors, several approaches are being investigated as potential means of sequestering and storing carbon dioxide. In the last 10 years, a great deal of research has been conducted on adsorbents such as metal-organic frameworks [5–7], zeolite [8–10], organic polymers [11–13], silica [14–16], and especially porous activated carbons (ACs) [17–19].

Activated carbons are without a doubt the most extensively investigated, incredibly effective, and frequently utilized adsorbent among CO_2 solid adsorbent materials. This is particularly vital when considering their exceptional textural characteristics, high surface area, tunable porosity, high degree of surface reactivity, good stability, and affordable low price for industrial applications [20]. The large internal surface area of AC is mainly due to the presence of micropores, whereas macropores act as a conduit through which adsorbate molecules can be transported to the micropores [21]. Most applications of activated carbons include

* Corresponding author.
E-mail address: jaroslaw.serafin@qi.ub.es (J. Serafin).

https://doi.org/10.1016/j.susmat.2023.e00717
Received 21 June 2023; Received in revised form 6 September 2023; Accepted 13 September 2023
Available online 17 September 2023

adsorption techniques for the purification of air (NO_X, SO_X, CH_4, and CO_2) and water (organic matter, pesticides, nitrates, metals, and dyes), as well as the recovery of volatile chemicals compounds (VOC) from gases [22]. They also have more limited use as catalysts, catalyst supports, supercapacitors, energy storage, and electrodes on a smaller scale [23]. However, the capture and storage of carbon dioxide must be considered first and foremost among the potential implementation on an industrial scale that may be developed and achieved at a high level of technological maturity. In recent years, significant progress has been made in activated carbon preparation, focusing on the optimization of various synthesis methods that can enhance its CO_2 capture performance. One key direction involves the use of advanced activation techniques, such as microwave or plasma activation, which have been developed to improve the porosity and surface area of AC materials [24,25]. Researchers are also exploring the creation of hybrid materials, which combine the advantages of ACs with other materials, such as metal-organic frameworks or graphene, to further enhance the CO_2 adsorption capacity and selectivity [26,27]. Furthermore, surface modification is another area of progress, with various techniques being developed to modify the surface of activated carbon and improve its CO_2 uptake performance, including impregnation with metal oxides [28].

Moreover, current research remains on investigating the use of novel precursors, mainly waste materials from industrial processes. The production of ACs is based on conventional carbonaceous raw materials rich in high carbon concentration and low inorganic content of both plant and industrial origins, such as hard coal, lignin, peat, wood, fruit stones or peat [29]. Hence, natural resources should be distinguished by high mechanical and thermal resistance, the highest concentration of elemental carbon, and a minimal quantity of volatile and inorganic elements. ACs may be manufactured from many raw materials, such as polymers, synthetic resins, or, especially, a variety of biomass. Utilizing waste biomass for AC production reduces the burden on landfills, considering abundant amounts of waste biomass from widely several sources, including agricultural leftovers, forestry waste, and even municipal solid waste. Furthermore, the literature has suggested that porous carbons obtained from biomass provide a promising opportunity for the sustainable and cost-effective production of adsorbents for CO_2 capture. Therefore, numerous investigations have recently been conducted using biomass-derived porous carbons [30,31,32] and their modification strategies, especially heteroatom doping [33], for CO_2 adsorption applications.

Those by-products are inexpensive and also easy to acquire, reduce the amount of transport needed if the product is located locally, offer a more environmentally friendly alternative, and simultaneously promote the reuse and recycling of organic materials that must be disposed of. In particular, olive stones, which are the hard, pit-like structures found inside olives, have become increasingly popular precursor materials in the European Union for the production of ACs. >2,6 million hectares are devoted to olive farming in Spain, where 6,2 million tons are produced annually. Of this amount, 420.000 tons of stones are produced, of which 323.500 tons are sold, making them significant materials for recycling [34]. In view of this, ACs have an exceptionally beneficial influence on the environment and contribute to the development and enhancement of the circular economy [35]. This is strictly associated with ecology in its broadest sense and is the task of properly managing the ever-increasing amount of wastes.

The characteristics of emerging carbon materials, principally the degree of porosity, are closely related to their structure, which is dictated by the type of initial precursors and the pyrolysis conditions [36]. Carbonization, also known as pyrolysis, is the first stage in the synthesis of ACs. It involves heating the raw material to a temperature of approximately 200 °C to remove significant amounts of moisture (H_2O). The material is then subjected to a thermal treatment at a temperature ranging from 500 to 700 °C, during which the removal of biological contaminants, tar, polymers, carbon dioxide, hydrocarbons and volatile organic chemicals takes place [37]. In addition to this, the pyrolysis procedure must be performed in accordance with certain process parameters, such as doing so in an atmosphere devoid of oxygen and the involvement of chemical agents [38]. Generally, the porosity of ACs obtained from this stage is inadequate for the vast majority of practical applications involving CO_2 capture due to the undeveloped microporosity and a small specific surface. Therefore, the generic synthesis of activated carbons is based on either one of two fundamental methods, physical activation or chemical activation. The final characteristics of activated carbon, such as the number of pores, surface area, and pore size distribution, are significantly influenced by the activation technique and process parameters that were examined [39].

The physical activation process can be done in a single or two steps. This means that raw material can be carbonized first and then simultaneously activated, or the resulting char from the carbonization step is collected and subjected to the activation process with oxidant gases such as steam, CO_2, or O_2 at temperatures between 600 and 1000 °C [40]. In chemical activation, the activating agent is impregnated or physically mixed with the starting material, followed by heating in an inert atmosphere at temperatures of 400–950 °C. Among the most widely utilized activating agents, they are classified into one of four categories: acidic, alkaline, and neutral metal salts and other catalysts. That is, among others, nitric acid (HNO_3), ferric chloride ($FeCl_3$), orthophosphoric acid (H_3PO_4), potassium carbonate (K_2CO_3), sodium hydroxide (NaOH), potassium hydroxide (KOH) and zinc chloride ($ZnCl_2$) [41]. The activating agents are then removed from the pores occupied by activated char by washing it with alkaline, acid, or water, and the product is separated from the slurry before being dried and conditioned [39].

However, chemical activation has one rather special disadvantage, namely the negative environmental impact of most of the activating agents and their subsequent disposal. For example, because KOH and NaOH are hazardous and toxic to both people and aquatic organisms at very low concentrations, it is imperative that their position as chemical agents be carefully evaluated in connection with the preservation of the environment. It may cause a destructive effect on nature, including long-term degradation, extreme ecotoxicity in the water environment, and finally mass mortality of birds, mammals, and other terrestrial organisms [42,43]. The same applies to other activating agents, which are dangerous, aggressive media and require additional precautions to be taken before the expanding chemical may be reclaimed for further activation work. Among acids, HNO_3, as an air pollutant, can contribute to a wide range of health concerns and unfavorable effects on the surrounding environment in the atmosphere, including ground-level ozone, acid rain, and vision impairment [44]. H_2SO_4 has a level of acute (short-term) toxicity that is moderate for aquatic organisms. Due to its high corrosiveness, sulfuric acid would cause severe damage to the tissues of any living organism exposed to it [45]. Furthermore, H_3PO_4 released into the environment can acidify both soil and water [46]. In the case of inorganic compound salt ($FeCl_3$, $ZnCl_2$), which are hazardous contaminants, they possess long-term detrimental impacts on aquatic ecosystems, soils, causing significant levels of heavy metal concentrations during discarding them without any prior treatment [47,48]. With the discussed problems considered, minimizing the harmful effects of chemical reagents on habitat and their proper disposal is one of the interesting directions of research in this field. Moreover, using innovative ecofriendly chemical agents would make it possible to eliminate any barrier that could be overcome.

Understanding AC risk and life-cycle assessment (LCA) is necessary for the valorization of AC through the CO_2 application pathway outlined before. This is primarily owing to the fact that environmental and economic considerations are at the forefront of this endeavor. Hence, in this work, we present a novel methodology for obtaining bioorganic activating agent from banana peels extract synthesis for activated carbon synthesis. Our way of producing ACs will not only lead to a significant reduction in the amount of dangerous waste after the chemical activation process and solving problems in the sense of their disposal but will

also allow them to transform those porous carbon-based materials into entirely environmentally friendly solid CO_2-adsorbents derived from biomass sources. The included approach depicts a global problem-solving approach that takes on issues such as climate change, the loss of biodiversity, waste, and pollution.

2. Materials and methods

2.1. Natural activator preparation

The banana peels used were washed steam with distilled water and dried in the dryer at 105 °C for 24 h to remove moisture and volatile impurities. Further, they were cut into small pieces and burnt in a horizontal oven at 300 °C for 1 h with air flow. The black powder obtained was collected and washed again with distilled water to remove the impurities present in the powder. Then, 1 mg/mL dispersion of synthesized black powder was prepared in water and further used as an activating agent (bioorganic KOH solution from banana extract) for producing activated carbon from olive stones. Fig. S1 shows a schematic preparation of the natural activator, and Table S1 presents the elemental composition, especially the potassium content of the banana extract. Moreover, the elemental analysis results of the ACs are presented in Table S2.

2.2. Preparation of activated carbons

The scheme for the preparation of activated carbon from olive stones is shown in Fig. 1. Initially, the olive stones were grounded, then dried at 105 °C and prepared as a precursor material for activated carbon. The chemical activators were saturated KOH solution, 85% H_3PO_4 and KOH solution from banana peels extract with 54.9% of potassium content, respectively. First, saturated KOH and 85% H_3PO_4 olive stones powder were treated with the activator at ambient temperature for 3 h. When used as a bioorganic activator, the KOH solution was added to the olive stones powder and stirred with a magnetic stirrer for 48 h. The weight ratio of each activator: precursor was 1:1. All materials were then carbonized in continuous N_2 gas at 18 L STP/min. A carbonization temperature of 500 °C was reached with a heating rate of 10 °C/min and held for 1 h. The selection of 500 °C as activation temperature was based on its well-established efficiency in previous biomass-to-activated carbons conversion studies. This temperature has been widely reported in the specific range as an effective and reliable choice for achieving the desired carbonization and activation processes.

After the activation process, to prevent oxidation, the samples were cooled in a furnace in a stream of N_2 gas. After cooling down, the obtained products activated with saturated KOH (KOH-AC) and 85% H_3PO_4 (H_3PO_4-AC) were washed with distilled water, then with hydrochloric acid at a concentration of 1 mol/dm^3 and again with distilled water until a neutral reaction was obtained. When a bioorganic KOH solution was used as an activator, the sample (BIO-AC) was washed with distilled water only till the moment when a neutral supernatant was obtained. The resulting material was finally dried in an oven at 200 °C overnight.

Additionally, it is important to provide a clear and detailed description of the chemical reactions involved in the preparation of porous materials using chemical reagents and active ingredients from banana peel. In the case of acidic treatment, as a result of the dehydration of H_3PO_4, water is liberated. Subsequently, the obtained P_4O_{10}, functioning as a robust oxidizing agent, engages with carbon to generate new pores while expanding existing ones. This reaction leads to the emission of carbon dioxide. The reactions occurring in activating biomass using phosphoric acid within defined temperature ranges are provided below [49]:

- At a temperature range of 100–400 °C

$$2H_3PO_4 \rightarrow H_4P_2O_7 + H_2O \quad (1)$$

$$3H_3PO_4 \rightarrow H_5P_3O_{10} + 2H_2O \quad (2)$$

$$nH_3PO_4 \rightarrow H_{n+2}P_nO_{3n+1} + (n-1) + 2H_2 \quad (3)$$

- At a temperature range of 400–700 °C

$$H_{n+2}P_nO_{3n+1} \rightarrow P_4O_{10} + H_2O \quad (4)$$

$$P_4O_{10} + 2C \rightarrow P_4O_6 + 2CO_2 \quad (5)$$

Furthermore, specific reactions between the biomass and KOH occurred during the carbonization combined with chemical activation. Carbon oxidation led to potassium carbonate, hydrogen, metallic potassium, water, and carbon oxide. The main reactions of biomass and KOH were as follows:

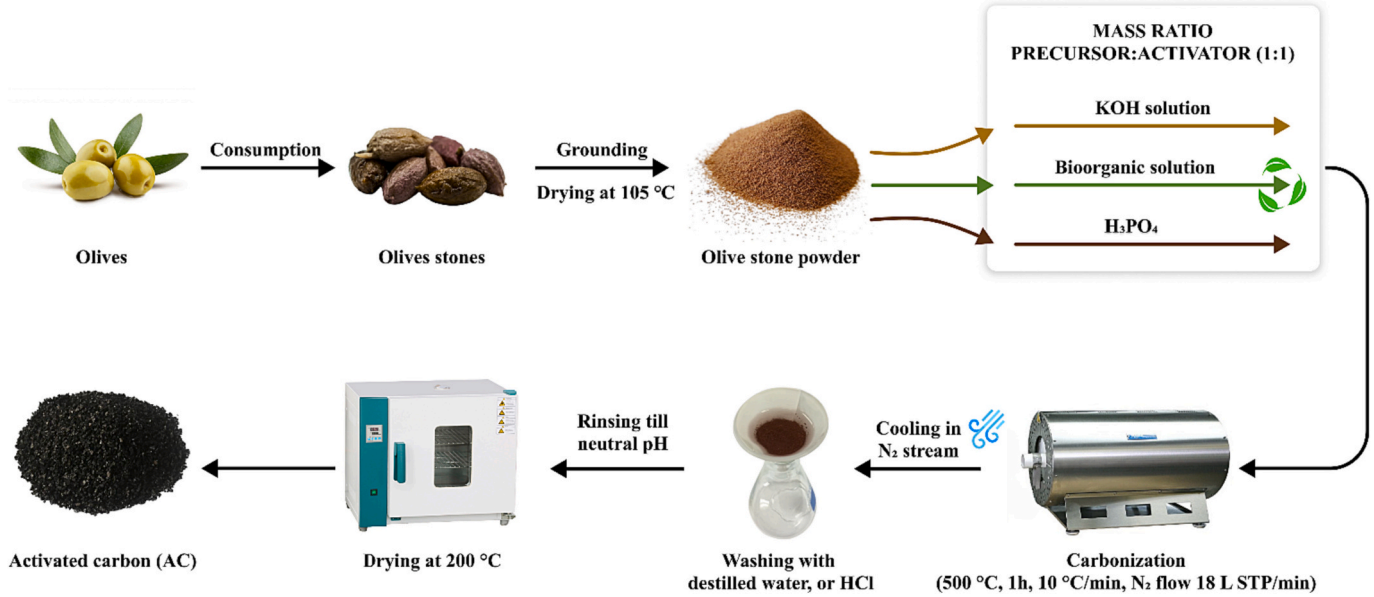

Fig. 1. Schematic preparation of activated carbon derived from olive stones.

$$4KOH + C \rightarrow K_2CO_3 + H_2O + 2H_2 \quad (6)$$

$$KOH + 2C \rightarrow 2K_2CO_3 + 2\,K + 3H_2 \quad (7)$$

$$KOH + C + H_2O \rightarrow K_2CO_3 + 2H_2 \quad (8)$$

$$KOH + 2C \rightarrow 2CO + 2\,K + H_2 \quad (9)$$

The chemical reactions using banana peel extract in the preparation of porous materials could involve the breakdown of biomass components and the interaction of their constituents with the active ingredients, regardless of the presence of KOH. Assuming the biomass contains cellulose as a major component and the active ingredients in banana peel extract consist of phenolic compounds, the reaction might proceed as follows:

- Hydrolysis of biomass (cellulose)

$$\text{Biomass (cellulose)} + \text{Water } (H_2O) \rightarrow \text{Glucose} + \text{Other sugars} \quad (10)$$

- Interaction with phenolic compounds from banana peel extract

$$\text{Glucose} + \text{Phenolic compounds} \rightarrow \text{Phenolic} - \text{glucose complexes} \quad (11)$$

Cellulose from the biomass undergoes hydrolysis in the presence of water to produce glucose and other sugars. This step involves the breakdown of cellulose into simpler sugar compounds. Further, the phenolic compounds from banana peel extract can react with the glucose and other sugars produced during biomass hydrolysis. These reactions can result in the formation of phenolic-glucose complexes or other chemical species, which may further react or undergo transformations to form the desired porous material.

2.3. Research methods

To determine the textural properties of synthesized AC samples, nitrogen adsorption/desorption isotherms at −196 °C and carbon dioxide at 0 °C were measured. This characterization of the porous structure was carried out on QUADRASORB evo™ gas sorption surface area and pore size analyzer. Prior to the measurements, all samples were degassed at 250 °C for 16 h. Using adsorption data at relative pressures ranging from 0.05 to 0.25, the conventional Brunauer-Emmett-Teller (BET) equation was applied to estimate the specific surface area (S_{BET}) of developed activated carbons. At the maximum relative pressure ($P/P_0 = 0.99$), the total pore volume (V_{tot}) was evaluated by using N_2 adsorption isotherms. The non-local density functional theory (NLDFT) model was employed in the method for determining the porosity of AC samples – pore size and pore size distributions (PSDs) from N_2 and CO_2 adsorption isotherm experimental data, at temperatures 196 °C and 0 °C, respectively. Specifically, the adsorption of carbon dioxide enabled to deeply study of microporosity with pore size ranges between 0.30 and 1.50 nm. Generally, the main aim of the NLDFT is to investigate the adsorption of spherical molecules in porous materials of any geometries.

The energy-dispersive X-ray fluorescence spectroscopy (EDXRF) was applied to measure the potassium quantity in the elemental composition of banana extract, as activating agent. Epsilon 3 spectrometers, manufactured by PANalytical B.*V.*, served as the instrumentation. Elemental analysis of activated carbons was conducted using elemental analyzers manufactured by LECO Corporation.

Phase analysis of the activated carbons was performed by XRD. Utilizing an X-ray diffractometer (PANalytical Empyrean) with Cu Kα radiation (λ) wellspring of 0.154 nm in the 2θ range of 20–80°, X-ray diffraction patterns of activated carbon from olive stones were recorded and analyzed.

The structure of the carbon skeleton of the obtained carbon materials was evaluated by using Raman spectroscopy. The tests were carried out with the assistance of a InVia Raman Microscope spectrometer, equipped with a laser inducting the AC samples at a wavelength of 785 nm. After the procedure of setting the highest of the G peak in each spectrum to 1, the intensity and location of the G and D peaks were detected, and the ratio of the intensities of these peaks was calculated.

Scanning electron microscopy (SEM) images of the surface morphologies as well as differences in the shapes of the surface of activated carbons were performed on an Ultra-high Resolution Scanning Electron Microscope Hitachi SU8000 with the EDS X-ray microanalyzer and cold emission (HITACHI UHR FE-SEM).

The volumetric sorption analyzer used to evaluate the N_2 adsorption isotherms (QUADRASORB evo™ gas volumetric apparatus) was also used to evaluate the CO_2 capture performance at ambient pressure. Measurements of CO_2 adsorption were carried out at two temperatures of 0 °C and 30 °C, throughout a pressure range of 0–1.0 bar in the presence of high-purity CO_2 (99.999%) that was supplied into the system. Before conducting the adsorption experiments, the carbon materials were degassed for 16 h at 200 °C under a vacuum to remove any moisture and gaseous pollutants. In the case of determining CO_2/N_2 selectivity, adsorption equilibrium tests were performed for a temperature of 30 °C.

3. Results and discussion

3.1. Porous characteristics of bioorganic AC

Investigations of N_2 adsorption and desorption at a temperature of −196 °C were used to analyze the textural characteristics of novel bioorganic activated carbon materials developed in this study. They are depicted schematically in Fig. 2a, which served as the basis for the analysis described below. According to the current International Union of Pure and Applied Chemistry (IUPAC) classification system of gas–solid adsorption isotherms from 2015, the BIO-AC and H_3PO_4-AC at low relative pressure values (approximately below $P/P_0 < 0.15$) represent Type I (a), as well as in the region spanning a moderate to higher range, Type IV [50]. Consequently, these characteristics indicate combination attributes of type I/IV related to a micro-mesoporous AC, with a severe heel before reaching 0.015 P/P_0 and a flat hysteresis loop at a relative pressure varying between 0.47 and 0.96 for BIO-AC and 0.1–0.96 for H_3PO_4-AC, respectively.

Furthermore, hysteresis loops can be indicated as Type H4, corresponding to slit-shaped micropores and a small quantity/size of mesopores in the internal structure of material [51,52]. The only thing worth highlighting is the low-pressure hysteresis of H_3PO_4-AC, which may be associated with the deformation of non-rigid pore walls or chemical adsorption [53]. On the other hand, the isotherms of activated carbon obtained from chemical activation via KOH seemed to initially overlap. However, Fig. S2 confirms the appearance of a loop at the magnification of the N_2 adsorption and desorption curves.

The logarithmic scale is commonly used to analyze isotherms because it provides a clearer view of the behavior of N_2 molecules entering the porous system at both low and high pressures, as shown in Fig. 2b. On a logarithmic scale, the region of low pressure appears as a straight line, indicating that N_2 molecules primarily interact with the surface through physical adsorption forces. This suggests that N_2 molecules are weakly adsorbed and do not occupy the porous structure significantly. As pressure increases, the isotherm starts to deviate from linearity, indicating the onset of multilayer adsorption. In this region, N_2 molecules begin to occupy the porous structure more efficiently, forming multiple layers on the surface. At high pressures, the isotherm approaches a plateau, indicating that most of the available adsorption sites are occupied, and further adsorption becomes limited.

Generally, Type I (a) of isotherm is characterized by high adsorption quality in the frequency range concentrations of adsorbate and the consuming plateau without the possibility of additional adsorption. Moreover, it is reported that narrow microporous adsorbents possessing small pores of <1 nm [50]. In the case of Type IV, it is strictly connected

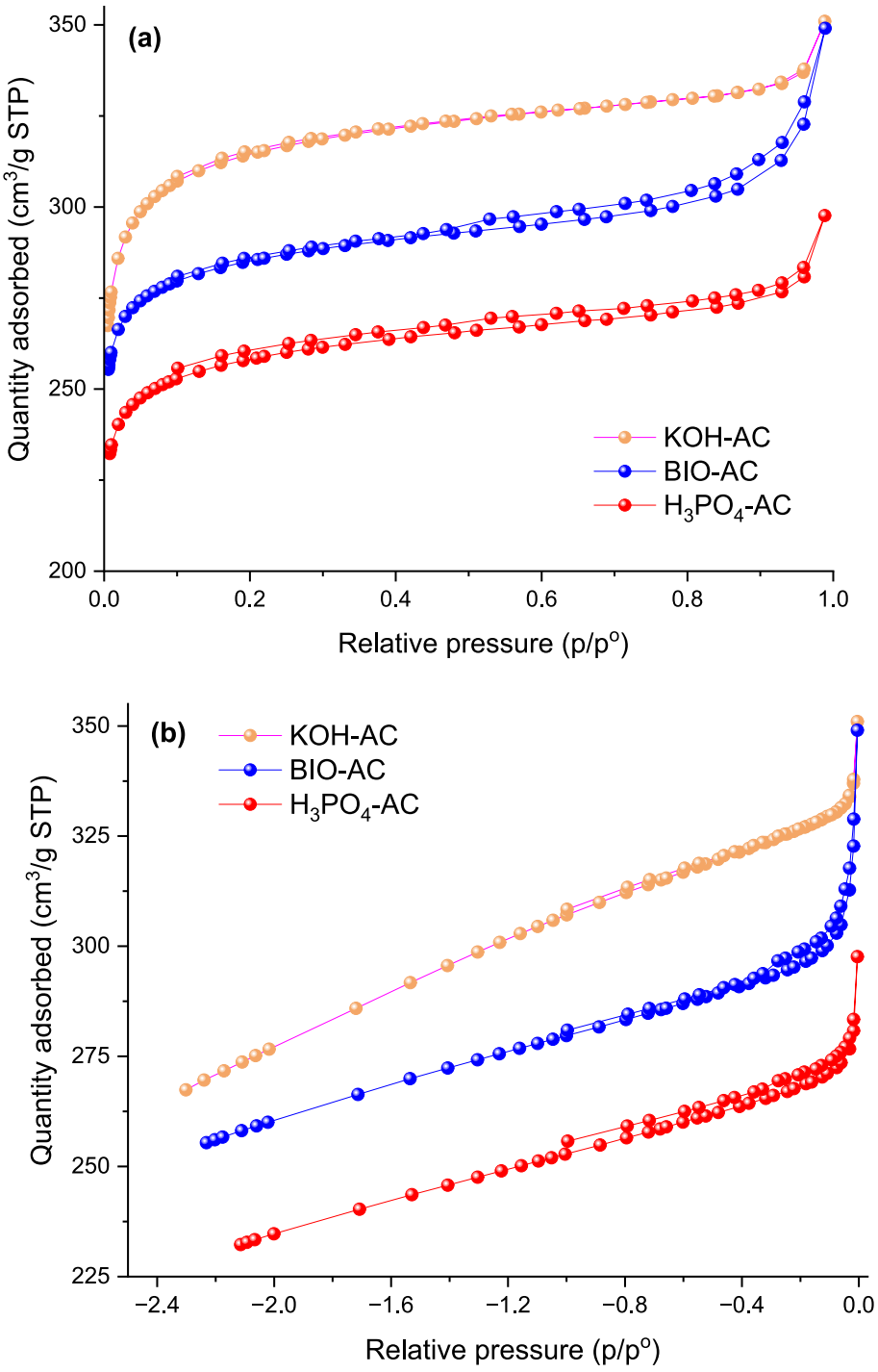

Fig. 2. N_2 adsorption-desorption curves of the AC samples at −196 °C (a), logarithmic-scale plot of N_2 adsorption (b).

because of capillary condensation taking place after multilayer adsorption in mesopores. Adsorption of gaseous molecules onto the walls of mesoporous materials results in the formation of a condensed adsorbed layer inside the mesopores as a reaction to the depression effect caused by the saturated vapor pressure of confined vapor [54].

The textural properties of AC obtained with a variety of chemical activating agents (KOH, bioorganic KOH, and H_3PO_4) are summarized in Table 1. The Brunauer-Emmett-Teller (BET) surface areas are relatively high, with the sample KOH-AC having the highest value of 969 m^2/g, a total pore volume of 0.544 cm^3/g, a micropore volume of 0.443 cm^3/g, and the number of micropores occupying the porous system reach 81.44%. The H_3PO_4-AC and BIO-AC were found to have a smaller BET

Table 1
Textural parameters of the bioorganic prepared activated carbons.

AC sample	Yield content [%]	BET surface area, m^2/g	Total pore volume, cm^3/g	Micropore volume, cm^3/g	Micropore content, %
KOH-AC	53.3	969	0.544	0.443	81.44
BIO-AC	58.8	915	0.495	0.444	89.69
H_3PO_4-AC	55.9	842	0.431	0.339	78.79

surface area varying from 842 to 915 m^2/g, a total pore volume of 0.431 to 0.495 cm^3/g, with a micropore volume oscillating between 0.339 and 0.444, respectively. Furthermore, the synthesized H_3PO_4-AC and BIO-AC samples also comprised mainly a proportion of microporosity, 78.79 and 89.69% of the porous structure. According to the findings, the use of a novel eco-friendly synthesis method of chemical activation leads to a more favorable environment for the pore expansion of AC and the development of microporosity. In particular, the utilization of potassium hydroxide as an activating agent has a favorable influence on the carbon skeleton, which may contribute to the creation of a large number of micropores and, consequently, a rise in specific surface area and total pore volume. This allows to provide of additional channels and surface active sites that are necessary for the diffusion and adsorption of gases.

Further, a non-local density functional theory (NLDFT) model was implemented in this work, based on the N_2 adsorption-desorption isotherm at −196 °C to determine the pore size distributions (PSD) of all AC samples. The obtained results were plotted in Fig. 3 (a). In accordance with the graph, most of the pores in KOH- AC, BIO-AC and H_3PO_4-AC are nearly entirely spread in the width range that is relatively concentrated within 4 nm. Based on the PSD curves for each of the samples, it can be noticeably concluded that the majority of pores fall within the microporosity spectrum along with a fewer number of mesopores of a comparatively small size. While the volume of micropore diameters is mostly focused between 1 and 1.5 nm, related to the two

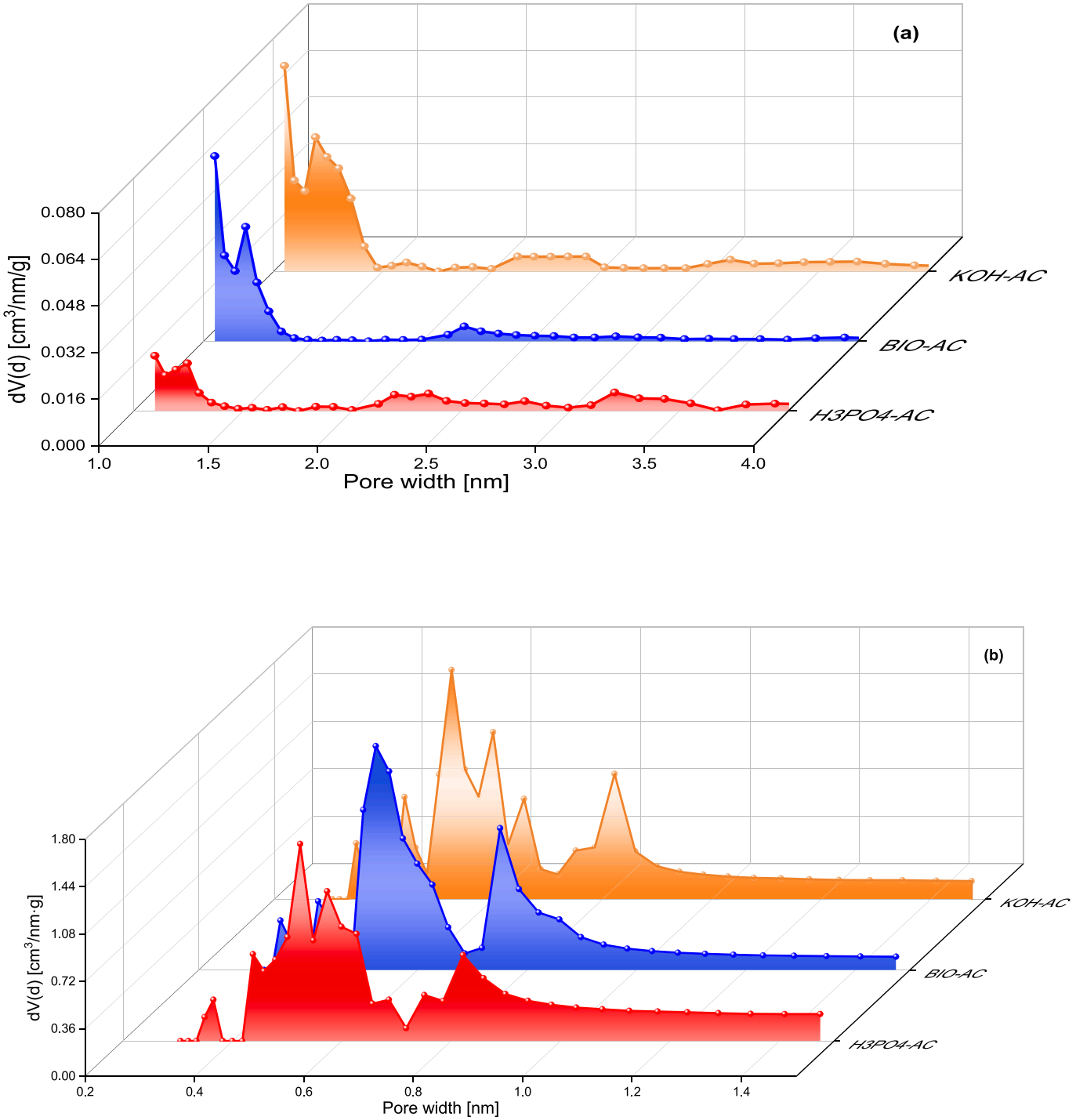

Fig. 3. Pore size distribution determined with the DFT method based on N_2 adsorption isotherm at −196 °C (a) and. CO_2 adsorption isotherm at 0 °C (b).

highest peaks at 1.05 nm and 1.2 nm; the mesopore diameters are largely centered in the range 2–4 nm, except BIO-AC fluctuates in 2–2.5 nm. It is observable that quite plainly activated carbon through KOH and H_3PO_4 possessed the largest micropore volume. In addition, KOH-AC contains mesopores, which proves the importance of an in-depth and comprehensive examination of PSD.

The micropore size distribution based on CO_2 adsorption at 0 °C was examined by applying the NLDFT method and is given in Fig. 3 (b), with a pore width between 0.30 and 1.50 nm. This approach allowed for a detailed analysis of pores classification in the microporous structure of ACs. The findings indicated that activation with saturated and bio-organic KOH solution especially favored the primarily creation of ultramicropores (<0.7 nm) and supermicropores (0.7–2 nm), in view of the highest three distinctive peaks in the diameter ranges from 0.40 to 0.46 nm, 0.48 to 0.69 nm and 0.72 to 0.90 nm of all three ACs samples, respectively. In the case of submicropores (<0.4 nm), another peak at a relatively low point on the graph can be also determined, occurring between 0.30 and 0.40 nm. Finally, Fig. 4 presents 3D simulation models of activated carbons obtained using the Avizo Software with the aim of visualizing the formation of the porous structure system.

The determination of activated carbon yield typically involves calculating the weight of activated carbon obtained after the activation and washing processes and then dividing it by the starting weight of the raw material. The activated carbon yield content varied between 53.3% and 58.8% as shown in Table 1. This calculation is performed on a dry basis, as shown by the following equation:

$$\text{Y content } (\%) = \frac{m}{m_0} \bullet 100 \quad (1)$$

The variables m and m_0 represent the dry weight of the final activated carbon (in grams) and the dry weight of the precursor (in grams), respectively.

3.2. Fourier-transform infrared spectroscopy (FTIR)

The surface functional groups of the BIO-AC and those treated with KOH-AC and H_3PO_4-AC were analyzed by Fourier Transform Infrared Spectroscopy (FTIR). The transmission method carried out the measurements with a sample dispersed in the KBr. The FTIR spectra were recorded in the wavenumber range from 4000 cm^{-1} to 500 cm^{-1}. As given in Fig. 5, the tested materials show a wide spectrum in the range of 3500–3450 cm^{-1} and a sharp band at 1385 cm^{-1} corresponding to O—H stretching vibrations that indicate the existence of free and intermolecularly bound hydroxyl groups [55]. A weak peak at 2755 cm^{-1} reveals that the carbons have a low content of aliphatic structures related to the presence of C—H stretching vibration [56,57,58]. Further, a peak between 2350 and 2420 cm^{-1} in a FITR spectrum can be attributed to the asymmetric stretching vibration of the CO_2 molecule, which is a characteristic vibrational mode used to identify the presence of CO_2 in a sample. The band at 1620 cm^{-1} can be identified as C═O aromatic structure stretching vibration [59]. The low band at the wavelength of about 825 cm^{-1} is associated with the presence of specifically the aromatic C═C stretching vibrations [55].

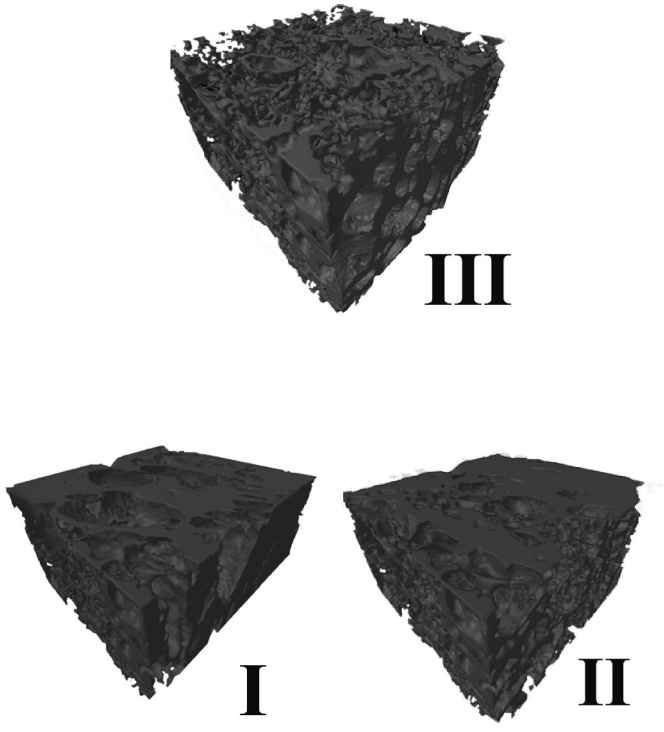

Fig. 4. Illustrative 3D representation of the microporosity, as well as the mesoporosity for H_3PO_4-AC (I), BIO-AC (II), and KOH-AC (III).

3.3. X-ray diffraction (XRD) method

The X-ray diffraction (XRD) method allowed the identification of the crystallographic characteristics and comprehending the structural features of the synthesized ACs. Fig. 6 illustrates the XRD patterns of BIO-AC, KOH-AC and H_3PO_4-AC, which substantiates the existence of crystalline structures of graphitic carbon. All samples roughly exhibit narrow and sharp diffraction peaks, and the lack of a wide peak indicates strong crystalline properties without a predominant amorphous phase [60]. According to the findings of the XRD analysis, the two diffraction peaks in the spectrum that emerged at angles 2θ equivalent to 24° and 44° are linked to the reflections that are found in the (002), and (100) crystal planes of aromatic layers in carbonaceous materials. The intensities of the H_3PO_4-AC (002) and (100) diffraction peaks are significantly higher than those of BIO-AC and KOH-AC. This suggests that the stacking structure of the aromatic layer has been considerably improved [61]. Moreover, (100) diffraction peak of BIO-AC is much smoother than others, which may determine that the crystallite size of KOH-AC and H_3PO_4-AC is quite larger [62].

3.4. Raman spectroscopy

The Raman spectra of all tested samples are shown in Fig. 7. The Raman spectra showed two typical bands in the range of about 1320 cm^{-1} (D-band) and 1596 cm^{-1} (G-band). Both D and G peaks are the result of vibrations of sp^2-bonded carbon atoms. The peak at the higher Raman shift is assigned to the G (Graphitic) band and is derived from stretching vibrations in the E_{2g} plane of all sp^2-bonded carbon atoms. The peak located at the lower Raman shift is assigned to the band D

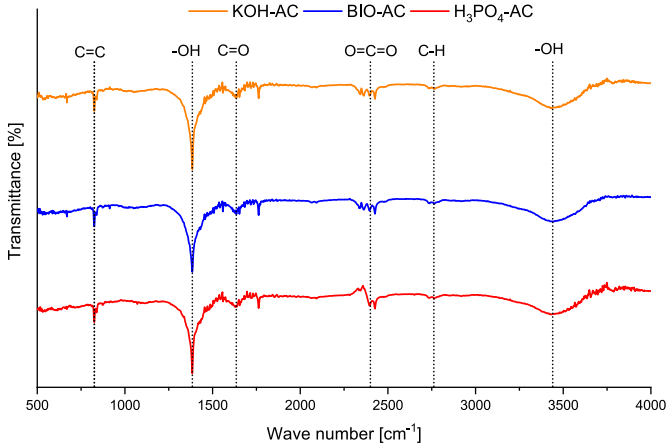

Fig. 5. FTIR spectra analysis of the obtained AC samples.

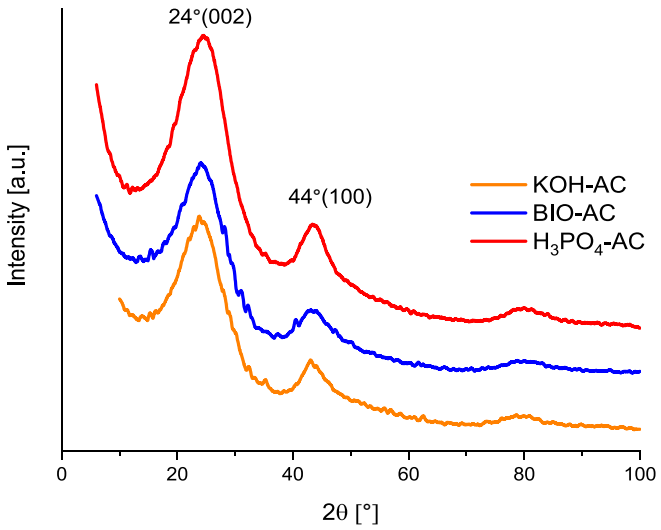

Fig. 6. The X-ray diffraction (XRD) spectra of the prepared AC samples.

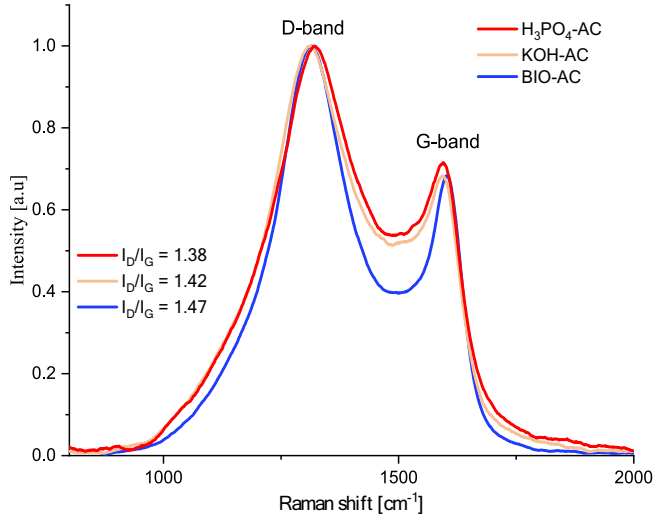

Fig. 7. Raman spectra of AC samples.

(Disorder) corresponding to the breathing vibrations with symmetry A_{1g} in the aromatic ring of carbons due to the presence of structural defects. It is a measure of the disorder of the close-range carbon structure [63,64,65].

The ratio of intensity I_D/I_G was used to determine the degree of disorder in carbon materials, allowing to estimate the degree of defects. The D/G ratio is related to the sp^3/sp^2 carbon ratio. If carbon material is fully oxidized, i.e., all carbon atoms are sp^3 hybridized, and if the D peak is higher, it indicates that the sp^2 bonds are broken, implying a greater presence of sp^3 bonds and a transition from sp^2 to sp^3 material, resulting in a maximum D/G ratio. The higher the I_D/I_G values, the more defects in the carbon structure and the lower the degree of graphitization [66]. The calculated I_D/I_G intensity ratio gradually increased from 1.38 for H_3PO_4-AC, 1.42 for KOH-AC to 1.47 for BIO-AC, which indicates the presence of more defects in the carbon skeletons and a greater degree of disorder. The higher I_D/I_G ratio for BIO-AC compared to the other carbons analyzed results in a relatively higher degree of disorder in the ordering of the carbon atoms, suggesting that more sp_2 domains are formed [67].

3.5. Scanning electron microscopy (SEM) analysis

To investigate the physical morphology of the surface and especially thoroughly examine the microstructure pores of ACs, a method known as scanning electron microscopy (SEM) was applied. Fig. 8 demonstrates the developed porous structure with a magnification of 5000–15,000× at a resolution of 1 μm, corresponding to the KOH-AC, BIO-AC, and H_3PO_4-AC samples, respectively. The rest of the SEM images with different magnification ranges (200–1500×) at results of 10 and 100 μm, are given in Fig. S3, Fig. S4 and Fig. S5. Based on SEM micrographs, it is noticeable that there is a discernible morphological difference between each other. As an outcome, pores of varying sizes and shapes become

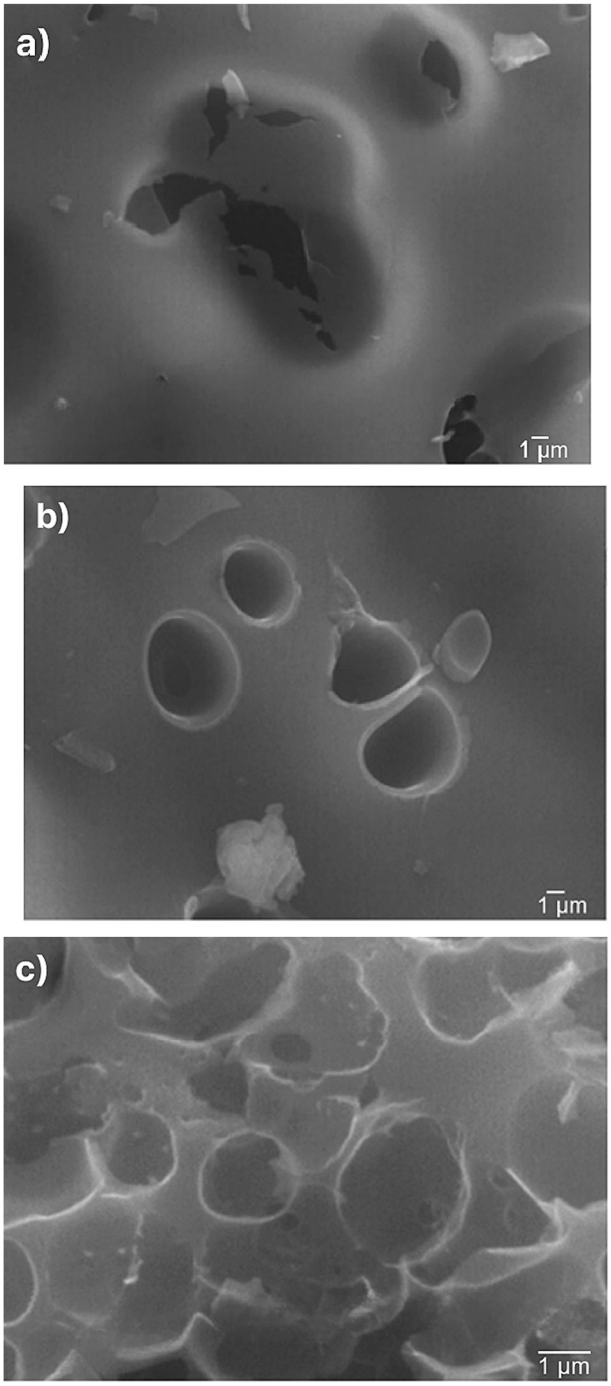

Fig. 8. Scanning electron microscopy (SEM) micrographs of the prepared KOH-AC (a), BIO-AC (b), and H_3PO_4-AC (c).

exposed for further observation. The skeletons of the samples appear to have a honeycomb structure (amorphous phase) with small grains on the AC surface that may be macropores linked directly to internal micropore channels, resulting in favorable sorption of CO_2 with high storage capacity and low transport resistance. Furthermore, by comparing three samples, chemical activation using KOH as the agent promotes the formation of micropores, which results in an increase in the total number of cavities (circular or elongated openings on the AC surface). The other two samples (BIO-AC and H_3PO_4-AC) have different microstructures that affect their sorption properties.

Upon comparison of the X-ray diffraction (XRD) results, it is evident that the substance exhibits a crystalline graphitic carbon structure, devoid of any amorphous phase. The Scanning Electron Microscopy (SEM) analysis exposed the amorphous phase of the material, showcasing its honeycomb mesh structure. There may be multiple factors contributing to these apparently inconsistent findings. It is plausible that the substance in question could comprise of both crystalline and amorphous components. The occurrence of mixed ordered and disordered structures is a prevalent phenomenon, as numerous materials exhibit this characteristic. The X-ray diffraction (XRD) analysis may have exclusively identified the crystalline phase, whereas the scanning electron microscopy (SEM) analysis disclosed the presence of the amorphous phase.

3.6. CO_2 capture capacity investigation

The CO_2 capture capacities of KOH-AC, BIO-AC, and H_3PO_4-AC were examined at two representative temperatures of 0 and 30 °C, under atmospheric pressure. Fig. 9 (a,b) illustrates a relative comparison of the CO_2 adsorption isotherms performance of as-prepared eco-friendly activated carbon samples. The CO_2 adsorption curves appear to be quite close to each other, with the only discernible variation being in the amount of CO_2 uptake. This observation is reasonable since the porous characteristics of each of these materials are analogous to one another (Table 1). Furthermore, analysis of the temperature influence plays an essential role in adsorption systems and determines whether physisorption or chemisorption is taking place. The amount of CO_2 adsorbed for all three AC samples decreases as the adsorption temperature rises. This implies an exothermic nature of the process on the activated carbon surface involving physical adsorption. The distance-dependent interaction between carbon dioxide molecules and AC solid sorbents has been greatly influenced by the importance of Van der Waals forces that have served in the adsorption mechanism. Higher temperature values simultaneously led to the instability of the adsorbate-adsorbent system by weakening the molecular bonding and promoting the process of desorption, which is a direct consequence of a change away from adsorption equilibrium in the reverse direction. Therefore, the adsorbed gas molecules possessed enough energy to overcome the weak attractive forces through the surface and migrate back into the gas phase.

The experimental results show that KOH-AC exhibits the highest CO_2 capture capacity of 6.32 mmol/g and 4.33 mmol/g at 0 °C, and 30 °C, due to the highest surface area and total pore volume. This demonstrates that the pore structure has a significant impact on CO_2 adsorption, even though the microporosity of KOH-AC (0.443 cm^3/g) is slightly lower than that of BIO-AC (0.444 cm^3/g). It is well known that micropores are primarily responsible for the adsorption of CO_2 in conditions of low pressure because the diameter of the molecules is equal to 0.33 nm. Interestingly, this observation can be associated with the presence of a certain number of mesopores that have the potential to enhance the usage of micropores and the CO_2 adsorption capacity of the material. When bioorganic KOH from banana peals extract and H_3PO_4 were used for the activation procedure, CO_2 uptake decreased to 6.00 and 5.44 mmol/g at 0 °C, under the same relative pressure value. At 30 °C, these values are equal to the following 4.00 and 3.59 mmol/g for BIO-AC and H_3PO_4-AC, respectively. In the case of H_3PO_4-AC, owing to the large volume of mesopores, which accounted for almost 80% of total pore

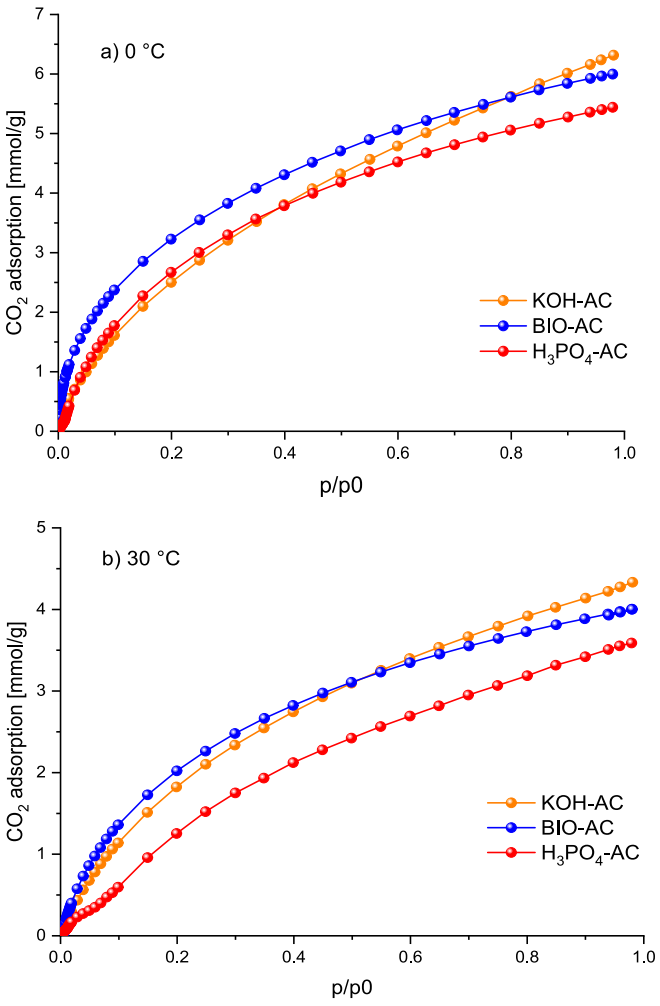

Fig. 9. CO_2 adsorption isotherms of KOH-AC, BIO-AC, and H_3PO_4-AC measured at (a) 0 °C and (b) 30 °C.

volume, the CO_2 adsorption capacity on the acquired carbon material was not particularly high. This was attributed to the reason that an excessive number of mesopores in the internal structure of a solid are claimed to be undesirable in the process of CO_2 capture. A diagrammatic illustration of the CO_2 adsorption mechanism in the porous structure of KOH-AC, BIO-AC, and H_3PO_4-AC is shown in Fig. 10, as the result of performing SEM analysis.

The final findings obtained are relatively high compared to those of other recently reported ACs. The CO_2 uptake of ACs made from various precursors at the temperature of 0, 25, and 30 °C is given in Table 2. Nevertheless, there hasn't been much research done on 30 °C, and most of those studies were performed below this value.

3.7. Isosteric heat of adsorption

This research study was to explore the isosteric heat of CO_2 adsorption (Q_{st}), which is a crucial metric to understand the adsorption behavior of the three synthesized activated carbon samples. Distinct patterns in the Q_{st} at different surface coverages were observed, providing insight into their distinctive adsorption properties, as shown in Fig. 11. The Q_{st} for the three samples falls within a range of approximately 48.35 kJ/mol to 11.95 kJ/mol, encompassing the different values observed for H3PO4-AC, BIO-AC, and KOH-AC at various surface coverages. Furthermore, it suggests that the adsorption mechanisms involved in these cases are more consistent with physical adsorption (20–40 kJ/mol) rather than chemisorption (80–200 kJ/mol), where

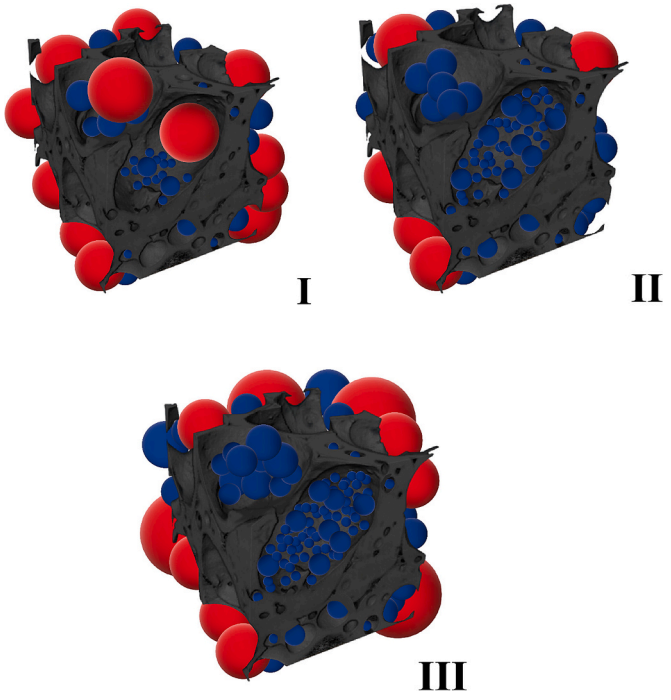

Fig. 10. Schematic illustration of the mechanism of CO_2 adsorption that occurs in the porous structure of H_3PO_4-AC (I), BIO-AC (II), and KOH-AC (III) (adsorption in mesopores – red color, and micropores – blue color).

Table 2
CO_2 adsorption capacity and CO_2 selectivity of various AC precursors at 1 bar and 0, 25, and 30 °C.

Carbon Source	0 °C (mmol/g)	25 °C (mmol/g)	30 °C (mmol/g)	CO_2 selectivity at 1 bar	Reference
Pomegranate peels	6.03	4.11	–	15.10	[68]
Bee-collected pollen	5.21	3.38	–	~15.00	[69]
Slash pine	4.93	–	–	–	[70]
Empty fruit bunch	5.20	3.71	–	11.20	[71]
Olive stones	2.84	1.98	–	–	[72]
Lumpy bracket	7.15	4.62	–	46.40	[73]
Packaging Waste	5.33	4.20	–	16.00	[74]
Common oak leader	6.17	5.44	–	74.36	[75]
Starch, cellulose, and sawdust	6.10	4.80	–	5.40	[76]
Hazelnut shell	6.34	4.23	–	19.00	[77]
Black lotus	7.21	5.05	–	30.75	[78]
Sugarcane bagasse	2.00	–	–	12.00	[79]
Coffee Grounds	4.40	3.00	–	18.00	[80]
Birch	4.50	4.06	–	93.10	[81]
Peanut shell char	7.25	4.41	–	7.90	[82]
Coconut shell	6.79	4.47	–	8.50	[83]
Water caltrop shell	6.06	4.22	–	19.00	[84]
Olive stones	6.32	–	4.33	161.1	This work

relatively weaker van der Waals forces and electrostatic interactions play a predominant role in the adsorption process [85].

A consistent finding among the three samples is that Q_{st} exhibits a decrease as surface coverage increases. The observed pattern implies a broad shift from more robust initial adsorption interactions to less strong ones, possibly indicating physisorption, as the adsorption sites reach saturation or as cooperative adsorption mechanisms become active with the gradual accumulation of CO_2 particles on AC surfaces. Consequently, adsorption becomes less energetically favorable, possibly due to the saturation of the adsorption sites or the influence of other competing interactions.

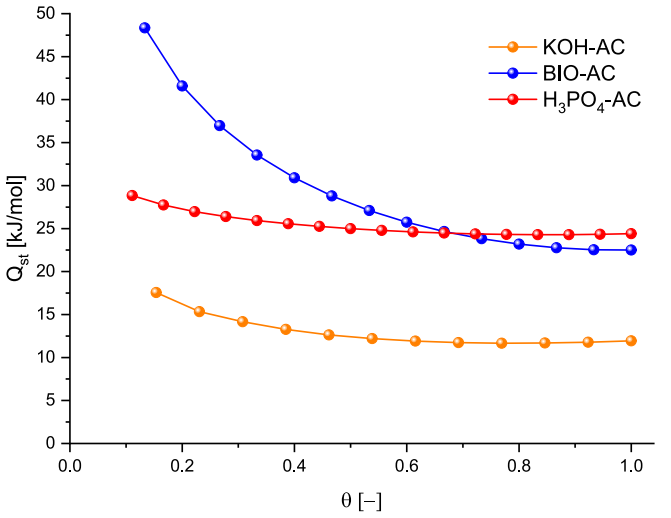

Fig. 11. Isosteric heat of adsorption of H_3PO_4-AC, BIO-AC, and KOH-AC as a function of surface coverage.

3.8. CO_2/N_2 selectivity studies

The selectivity of an adsorbent material for CO_2 over N_2 is an important factor for various environmental, industrial, and economic reasons during the CO_2 capture process. Hence, a measurement of nitrogen adsorption was additionally carried out on the BIO-AC sample, as a novel bioorganic activated carbon, at a temperature of 30 °C and 1 bar. The BIO-AC recovered from olivine stones possessed a maximum N_2 uptake of <0.141 mmol/g (Fig. S6). On the foundation of the CO_2 and N_2 adsorption isotherms at 30 °C, a complex examination of CO_2 over N_2 selectivity was further performed. In this study, the gas selectivity of CO_2/N_2 was calculated by employing the ideal adsorption solution theory (IAST) to accurately predict the separation efficiency.

The IAST method of Myers and Prausnitz has been widely used for estimating the adsorption selectivity of gaseous mixtures on porous materials. It assumes that the mixed-gas adsorption isotherm can be examined by combining the single isotherm of pure components [86,87] in accordance with the following equation of state:

$$S_{IAST} = \frac{q_{CO_2(p)}}{q_{N_2(p)}} \bullet \frac{p_{N_2}}{p_{CO_2}} \quad (2)$$

where: S_{IAST} is the selectivity coefficient, $q_{CO2(p)}$ and $q_{N2(p)}$ refer to the uptake of specific gas [mmol/g], p_{N2} and p_{CO2} are the partial pressure in the mixture.

Consequently, we examined the selectivity for CO_2/N_2 (0.5/0.5) binary mixture, where eq. (2) takes the below form:

$$S_{IAST(EQ)} = \frac{q_{CO_2(p)}}{q_{N_2(p)}} \quad (3)$$

Moreover, it is extremely valuable to examine the selectivity for flue gas compositions corresponding to those emitted directly from the industry. The content of flue gas depends on several factors, including the type of fuel used, the combustion process, and any treatment or cleanup systems in place. However, it is a well accepted fact that the flue gases for the most mature CO_2 capture technology (post-combustion capture) typically contain around 10–15% CO_2 and 75–80% N_2, along with other

gases such as oxygen, carbon monoxide, and sulfur dioxide. Further based on the IAST approach, the theoretical adsorption selectivity was also determined for the standard composition of flue gas (15% CO_2, 85% N_2), utilizing the following formula:

$$S_{IAST(FG)} = \frac{q_{CO_2(p)}}{q_{N_2(p)}} \bullet \frac{0.85}{0.15} \quad (4)$$

The selectivity obtained from IAST for an equimolar and flue gas CO_2/N_2 binary mixture at 30 °C is presented in Fig. 12. A significant decrease in the CO_2/N_2 selectivity ratio for both tested gas compositions can be observed up to 0.2 bar. In the case of 50% CO_2 and 50% N_2 mixture, the coefficient of adsorption selectivity of CO_2 over N_2 ranged from 422.8 to 28.4, depending on the change in pressure – as it is increased from 0.01 to 1 bar. Whereas for the gaseous content of 15% CO_2 and 85% N_2, the value of the CO_2/N_2 selectivity at a pressure of 0.01 bar was the highest (1442), while with increasing pressure, it decreased and ultimately achieved the lowest value of 161.1 for a pressure of 1 bar. A comparable trend has been described by us in many studies on CO_2 over N_2 selectivity [88,89]. In particular, it is important to note that the calculated S_{IAST} is among the highest reported in the scientific literature to date (Table 2).

The reason for such a high selectivity of CO_2/N_2 adsorption can be related to possessing a high surface area and a narrow distribution of pore size tend to demonstrate elevated selectivity value, as the adsorption of CO_2 is more favorable in smaller pores owing to its larger molecular size relative to N_2. Finally, the final findings show that AC derived from olive stones after subsequent activation with bioorganic KOH is an experimental direction that has the potential to create efficient sorbents for CO_2 capture on a commercial scale. In addition to the insights provided by results regarding the pressure-dependent selectivity of the tested adsorbent material for CO_2 over N_2, this study highlights the importance of understanding the behavior of adsorbent materials under various gas compositions, which can aid in the design and optimization of efficient CO_2 separation processes.

3.9. Stability evaluation of CO_2 capture

The stability of solid sorbent after many adsorption-desorption cycles under various operating conditions is an important consideration in designing efficient and cost-effective carbon capture technologies. It can directly affect the adsorption capacity and overall durability of the material, which are critical factors in determining its suitability and lifespan for commercial or industrial applications. Furthermore, the ability to maintain a constant adsorption capacity is critical for the economic viability of an adsorbent, as any decrease in performance or capacity can result in higher operating costs and lower capture efficiency. Consequently, by conducting fifty adsorption-desorption runs at 30 °C, the potential of the BIO-AC to be utilized repeatedly was assessed. To visualize the changes in adsorption capacity over successive cycles, the adsorption isotherms for the 1st, 5th, 10th, 20th, and 50th cycles were depicted in Fig. 13. The CO_2 adsorption performance of the BIO-AC remained constant even after undergoing fifty cycles, indicating its remarkable stability. The maximum standard deviation for among every runed cycles equals 0.05. This suggest that it is feasible to regenerate and reuse the material without any significant loss in its CO_2 uptake. Finally, it can be concluded that BIO-AC sample fulfills the standards of a desirable CO_2 sorbent, specifically with regard to its capacity for regeneration.

4. Conclusions

This work provides three different processes for the preparation of activated carbon using KOH saturated solution, H_3PO_4 acid and bioorganic KOH solution based on olive stone waste. The obtained results show that the physicochemical characterization of the prepared activated carbons, both with the participation of the saturated solution of KOH and the bioorganic KOH solution, are relatively similar to each other. AC synthesized by natural activating agent possessed well-developed specific surface area, the total pore volume and micropore volume that were 915 m^2/g, 0.495 cm^3/g and 0.444 cm^3/g, respectively. At the same time, it is worth emphasizing that the obtained bioorganic activated carbon was characterized by high sorption capacity, which was 6.32 mmol/g and 4.33 mmol/g, respectively for 0 °C and 30 °C. BIO-AC sample also exhibited high CO_2/N_2 selectivity of 161.1 for flue gas composition mixture and excellent stability over many adsorption-desorption cycles. Moreover, applying as an activated agent banana plant extract) bioorganic KOH solution), does away with the requirement for using any hazardous inorganic activating agent like acids or bases. What makes this method simple and easy. The synthesized activated carbon has possessed high porosity and adsorption stability. Thus, are successful in the green synthesis of activated carbon from wastes by avoiding toxic chemicals and using plant materials as an organic activating agent for the first time.

CRediT author statement:

J. Serafin: Conceptualization, Methodology, *V*alidation, Formal analysis, Investigation, Data Curation, Writing - Original Draft, Writing – review & editing, Project administration, Supervision.

B. Dziejarski: Methodology, Validation, Software, Formal analysis, Investigation, Data Curation, Writing - Original Draft, Writing – review

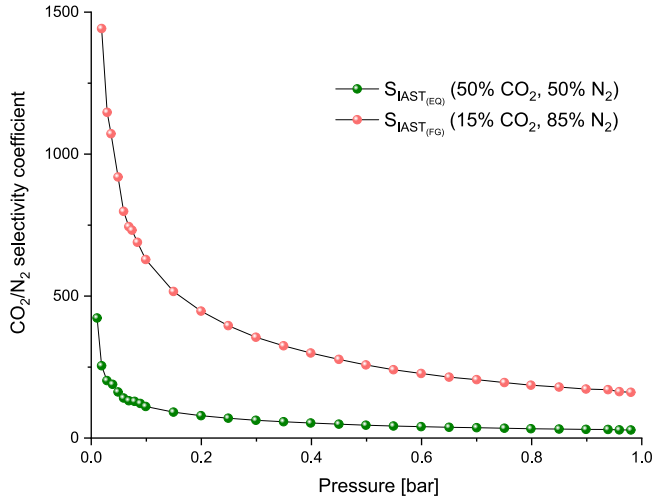

Fig. 12. CO_2/N_2 selectivity of BIO-AC versus pressure at 30 °C.

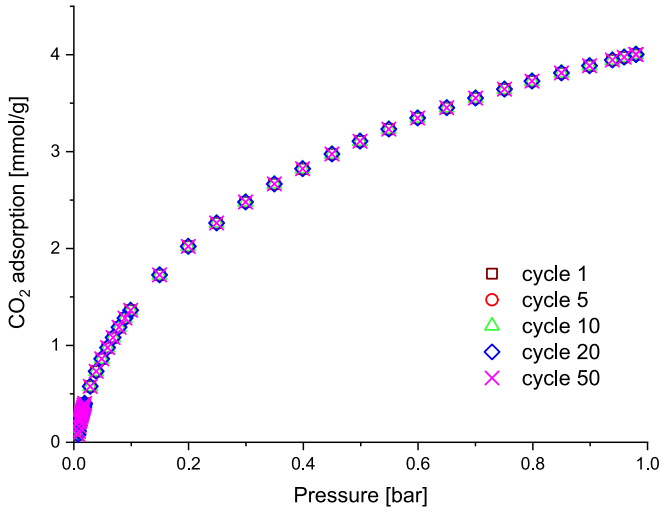

Fig. 13. CO_2 adsorption isotherms for BIO-AC at 30 °C in 1st, 5th, 10th, 20th, and 50th cycles.

& editing.

J. Sreńscek-Nazzal: Methodology, *V*alidation, Formal analysis, Investigation, Writing - Original Draft.

Declaration of Competing Interest

None.

Data availability

The data that has been used is confidential.

Acknowledgements

Jarosław Serafin is grateful to Spanish Ministry of Research and Innovation project no: PID2020-116031RBI00/AEI/10.13039/501100011033/FEDER

Appendix A. Supplementary data

Supplementary data to this article can be found online at https://doi.org/10.1016/j.susmat.2023.e00717.

References

[1] B. Dziejarski, R. Krzyżyńska, K. Andersson, Current status of carbon capture, utilization, and storage technologies in the global economy: a survey of technical assessment, Fuel 342 (127) (2023) 776.
[2] R.D. Piacentini, A.S. Mujumdar, Climate change and drying of agricultural products, Dry. Technol. 27 (2009) 629–635.
[3] IPCC, Summary for Policymakers, in: H.-O. Pörtner, D.C. Roberts, E.S. Poloczanska, K. Mintenbeck, M. Tignor, A. Alegría, M. Craig, S. Langsdorf, S. Löschke, V. Möller, A. Okem (Eds.), Climate Change 2022: Impacts, Adaptation and Vulnerability. Contribution of Working Group II to the Sixth Assessment Report of the Intergovernmental Panel on Climate Change, Cambridge University Press, Cambridge, UK and New York, NY, USA, 2022, pp. 3–33, https://doi.org/10.1017/9781009325844.001.
[4] IEA, Global Energy Review: CO2 Emissions in 2021, IEA, Paris, 2022 https://www.iea.org/reports/global-energy-review-co2-emissions-in-2021-2.
[5] J. Yang, Y. Wang, L. Li, Z. Zhang, J. Li, Protection of open-metal *V* (III) sites and their associated CO2/CH4/N2/O2/H2O adsorption properties in mesoporous V-MOFs, J. Colloid Interface Sci. 456 (2015) 197–205.
[6] S.E.M. Elhenawy, M. Khraisheh, F. AlMomani, G. Walker, Metal-organic frameworks as a platform for CO2 capture and chemical processes: adsorption, membrane separation, catalytic-conversion, and electrochemical reduction of CO2, Catalysts 10 (11) (2020) 1293.
[7] H. Furukawa, N. Ko, Y.B. Go, N. Aratani, S.B. Choi, E. Choi, O.M. Yaghi, Ultrahigh porosity in metal-organic frameworks, Science 329 (5990) (2010) 424–428.
[8] D. Panda, E.A. Kumar, S.K. Singh, Introducing mesoporosity in zeolite 4A bodies for Rapid CO2 capture, J. CO2 Utilizat. 40 (2020) 101,223.
[9] A.A. Dabbawala, I. Ismail, B.V. Vaithilingam, K. Polychronopoulou, G. Singaravel, S. Morin, Y. Al Wahedi, Synthesis of hierarchical porous Zeolite-Y for enhanced CO2 capture, Microporous Mesoporous Mater. 303 (110) (2020) 261.
[10] Q. Liu, P. He, X. Qian, Z. Fei, Z. Zhang, X. Chen, Y. Shi, Enhanced CO2 adsorption performance on hierarchical porous ZSM-5 zeolite, Energy Fuel 31 (12) (2017) 13933–13941.
[11] L. Wang, W. Xie, G. Xu, S. Zhang, C. Yao, Y. Xu, Synthesis of thiophene-based conjugated microporous polymers for high iodine and carbon dioxide capture, Polym. Adv. Technol. 33 (2) (2022) 584–590.
[12] C. Xu, Y. Zhu, C. Yao, W. Xie, G. Xu, S. Zhang, Y. Xu, Facile synthesis of tetraphenylethene-based conjugated microporous polymers as adsorbents for CO 2 and organic vapor uptake, New J. Chem. 44 (2) (2020) 317–321.
[13] D. Cui, C. Yao, Y. Xu, Conjugated microporous polymers with azide groups: a new strategy for postsynthetic fluoride functionalization and effectively enhanced CO 2 adsorption properties, Chem. Commun. 53 (83) (2017) 11422–11425.
[14] W.J. Son, J.S. Choi, W.S. Ahn, Adsorptive removal of carbon dioxide using polyethyleneimine-loaded mesoporous silica materials, Microporous Mesoporous Mater. 113 (1–3) (2008) 31–40.
[15] M. Ojeda, M. Mazaj, S. Garcia, J. Xuan, M.M. Maroto-Valer, N.Z. Logar, Novel amine-impregnated mesostructured silica materials for CO2 capture, Energy Procedia 114 (2017) 2252–2258.
[16] J. Jiao, J. Cao, Y. Xia, L. Zhao, Improvement of adsorbent materials for CO2 capture by amine functionalized mesoporous silica with worm-hole framework structure, Chem. Eng. J. 306 (2016) 9–16.
[17] M.G. Plaza, C. Pevida, B. Arias, M.D. Casal, C.F. Martín, J. Fermoso, J.J. Pis, Different approaches for the development of low-cost CO 2 adsorbents, J. Environ. Eng. 135 (6) (2009) 426–432.
[18] M.S. Shafeeyan, W.M.A.W. Daud, A. Houshmand, A. Arami-Niya, Ammonia modification of activated carbon to enhance carbon dioxide adsorption: effect of pre-oxidation, Appl. Surf. Sci. 257 (9) (2011) 3936–3942.
[19] E. Mehrvarz, A.A. Ghoreyshi, M. Jahanshahi, Surface modification of broom sorghum-based activated carbon via functionalization with triethylenetetramine and urea for CO2 capture enhancement, Front. Chem. Sci. Eng. 11 (2) (2017) 252–265.
[20] G. Singh, et al., Biomass derived porous carbon for CO2 capture, Carbon 148 (2019) 164–186.
[21] J. Serafin, B. Dziejarski, Activated carbons—preparation, characterization and their application in CO2 capture: a review, Environ. Sci. Pollut. Res. (2023) 1–55.
[22] P. Ammendola, F. Raganati, R. Chirone, CO2 adsorption on a fne activated carbon in a sound assisted fuidized bed: Termodynamics and kinetics, Chem. Eng. J. 322 (2017) 302–313.
[23] M.F.R. Pereira, J.J.M. Orfao, J.L. Figueiredo, Oxidative dehydrogenation of ethylbenzene on activated carbon catalysts. I. Influence of surface chemical groups, Appl. Catal. A Gen. 184 (1) (1999) 153–160.
[24] P. Kuptajit, N. Sano, K. Nakagawa, T. Suzuki, A study on pore formation of high surface area activated carbon prepared by microwave-induced plasma with KOH (MiWP-KOH) activation: effect of temperature-elevation rate, Chem. Eng. Process. Process Intensificat. 167 (108) (2021) 511.
[25] P.N.Y. Yek, R.K. Liew, M.S. Osman, C.L. Lee, J.H. Chuah, Y.K. Park, S.S. Lam, Microwave steam activation, an innovative pyrolysis approach to convert waste palm shell into highly microporous activated carbon, J. Environ. Manag. 236 (2019) 245–253.
[26] F.E. Che Othman, N. Yusof, M. Petrů, N.A.H. Md Nordin, M.F. Hamid, A.F. Ismail, S. Abu Hassan, Polyethyleneimine-impregnated activated carbon nanofiber composited graphene-derived rice husk char for efficient post-combustion CO2 capture, Nanotechnol. Rev. 11 (1) (2022) 926–944.
[27] S. Kayal, A. Chakraborty, Activated carbon (type Maxsorb-III) and MIL-101 (Cr) metal organic framework based composite adsorbent for higher CH4 storage and CO2 capture, Chem. Eng. J. 334 (2018) 780–788.
[28] A. Ghaemi, H. Mashhadimoslem, P. Zohourian Izadpanah, NiO and MgO/activated carbon as an efficient CO2 adsorbent: characterization, modeling, and optimization, Int. J. Environ. Sci. Technol. 19 (2) (2022) 727–746.
[29] H. Marsh, F. Rodriguez-Reinoso, Activated Carbon, Elsevier, Amsterdam, 2006.
[30] J. Bai, J. Huang, Q. Yu, M. Demir, M. Kilic, B.N. Altay, L. Wang, N-doped porous carbon derived from macadamia nut shell for CO2 adsorption, Fuel Process. Technol. 249 (107) (2023) 854.
[31] C. Ma, J. Bai, M. Demir, X. Hu, S. Liu, L. Wang, Water chestnut shell-derived N/S-doped porous carbons and their applications in CO2 adsorption and supercapacitor, Fuel 326 (125) (2022) 119.
[32] J. Serafin, B. Dziejarski, X. Vendrell, K. Kiełbasa, B. Michalkiewicz, Biomass waste fern leaves as a material for a sustainable method of activated carbon production for CO2 capture, Biomass Bioenergy 175 (106) (2023) 880.
[33] J. Shao, C. Ma, J. Zhao, L. Wang, X. Hu, Effective nitrogen and sulfur co-doped porous carbonaceous CO2 adsorbents derived from amino acid, Colloids Surf. A Physicochem. Eng. Asp. 632 (127) (2022) 750.
[34] https://expobiomasa.com/en/content/the-sales-of-the-olive-bone-as-biofuel-amount-more-than-50-million-euros.
[35] S. Nanda, A.K. Dalai, F. Berruti, J.A. Kozinski, Biochar as an exceptional bioresource for energy, agronomy, carbon sequestration, activated carbon and specialty materials, Waste Biomass Valorizat. 7 (2) (2016) 201–235.
[36] H. Benaddi, D. Legras, J.N. Rouzaud, F. Beguin, Influence of the atmosphere in the chemical activation of wood by phosphoric acid, Carbon (New York, NY) 36 (3) (1998) 306–309.
[37] P.R. Yaashikaa, P.S. Kumar, S. Varjani, A. Saravanan, A critical review on the biochar production techniques, characterization, stability and applications for circular bioeconomy, Biotechnol. Rep. 28 (2020), e00570.
[38] M. Tripathi, J.N. Sahu, P. Ganesan, Effect of process parameters on production of biochar from biomass waste through pyrolysis: A review, Renew. Sust. Energ. Rev. 55 (2016) 467–481.
[39] M.A. Yahya, Z. Al-Qodah, C.W.Z. Ngah, Agricultural bio-waste materials as potential sustainable precursors used for activated carbon production: a review, Renew. Sustain. Energy Rev. 46 (2015) 218–235. Available: DOI: https://doi.org/10.1016/j.rser.2015.02.051. ISSN 1364–0321.
[40] O. Ioannidou, A. Zabaniotou, Agricultural residues as precursors for activated carbon production—a review, Renew. Sust. Energ. Rev. 11 (2007) 1966–2005.
[41] H. Jankowska, A. Swiatkowski, A. Świątkowski, J. Choma, Active carbon, Ellis Horwood Limited, 1991.
[42] https://www.oxy.com/globalassets/documents/chemicals/stewardship/potassium-hydroxide.pdf.
[43] https://www3.epa.gov/pesticides/chem_search/reg_actions/reregistration/fs_PC-075603_1-Sep-92.pdf.
[44] X. Zhao, Z. Teng, J. Wang, X. Ma, Y. Sun, R. Gao, W. Wang, Barrierless HNO3 formation from the hydrolysis reaction of NO2 with Cl atom in the atmosphere, Atmos. Environ. 270 (118) (2022) 871.
[45] https://www.dcceew.gov.au/environment/protection/npi/substances/fact-sheets/sulfuric-acid.
[46] https://www.dcceew.gov.au/environment/protection/npi/substances/fact-sheets/phosphoric-acid.
[47] R.B. Sotero-Santos, O. Rocha, J. Povinelli, Toxicity of ferric chloride sludge to aquatic organisms, Chemosphere 68 (4) (2007) 628–636.
[48] X. Zhang, L. Yang, Y. Li, H. Li, W. Wang, B. Ye, Impacts of lead/zinc mining and smelting on the environment and human health in China, Environ. Monit. Assess. 184 (4) (2012) 2261–2273.

[49] I. Neme, G. Gonfa, C. Masi, Activated carbon from biomass precursors using phosphoric acid: a review e11940, Heliyon (2022) 11940.
[50] M. Thommes, K. Kaneko, A.V. Neimark, J.P. Olivier, F. Rodriguez-Reinoso, J. Rouquerol, K.S. Sing, Physisorption of gases, with special reference to the evaluation of surface area and pore size distribution (IUPAC Technical Report), Pure Appl. Chem. 87 (9–10) (2015) 1051–1069.
[51] J. Serafin, B. Dziejarski, Application of isotherms models and error functions in activated carbon CO2 sorption processes, Microporous Mesoporous Mater. 354 (112) (2023) 513.
[52] Y.C. Chiang, P.C. Chiang, C.P. Huang, Effects of pore structure and temperature on VOC adsorption on activated carbon, Carbon 39 (4) (2001) 523–534.
[53] G. Marcì, L. Palmisano (Eds.), Heterogeneous Photocatalysis: Relationships with Heterogeneous Catalysis and Perspectives, Elsevier, 2019.
[54] J. Reedijk, K. Poeppelmeier, Comprehensive inorganic chemistry II: from elements to applications, in: V1 Main-Group Elem., Incl. Noble Gases V2 Transition Elem., Lanthanides and Actinides V3 Bioinorganic Fundam. and Appl.: Metals in Nat. Living Syst. and Metals in Toxicology and Med. V4 Solid-State Mater., Incl. Ceramics and Minerals V5 Porous Mater. and Nanomaterials V6 Homogeneous Catal. Appl. V7 Surf. Inorganic Chem. and Heterog. Catal. V8 Coord. and Organometallic Chem. V9 Theory and Methods, Elsevier Ltd., 2013, pp. 1–7196.
[55] N.M. Ofgea, A.M. Tura, G.M. Fanta, Activated carbon from H3PO4 -activated Moringa Stenopetale Seed Husk for removal of methylene blue: Optimization using the response surface method (RSM), Environ. Sustainabil. Indicat. 16 (2022), 100214.
[56] I. Neme, G. Gonfa, C. Masi, Preparation and characterization of activated carbon from castor seed hull by chemical activation with H3PO4, Results Mater. 15 (2022), 100304.
[57] G. Tzvetkov, S. Mihaylova, K. Stoitchkova, P. Tzvetkov, T. Spassov, Mechanochemical and chemical activation of lignocellulosic material to prepare powdered activated carbons for adsorption applications, Powder Technol. 299 (2016) 41–50.
[58] E.R. Raut, M.A. Bedmohata, A.R. Chaudhari, Comparative study of preparation and characterization of activated carbon obtained from sugarcane bagasse and rice husk by using H3PO4 and ZnCl2, Mater. Today: Proceed. 66 (2022) 1875–1884.
[59] E.M. Mistar, T. Alfatahb, M.D. Supardanc, Synthesis and characterization of activated carbon from *Bambusa vulgaris* striata using two-step KOH activation, J. Mater. Res. Technol. (2020) 6278–6286.
[60] S. Wang, G.Q. Lu, Effects of oxide promoters on metal dispersion and metal–support interactions in Ni catalysts supported on activated carbon, Ind. Eng. Chem. Res. 36 (12) (1997) 5103–5109.
[61] T. Qiu, J.G. Yang, X.J. Bai, Y.L. Wang, The preparation of synthetic graphite materials with hierarchical pores from lignite by one-step impregnation and their characterization as dye absorbents, RSC Adv. 9 (22) (2019) 12737–12746.
[62] Z. Xie, W. Guan, F. Ji, Z. Song, Y. Zhao, Production of biologically activated carbon from orange peel and landfill leachate subsequent treatment technology, J. Chem. (2014) 2014.
[63] Seo Hui Kang, Ji Su Chae, Jung-Min Choi, Yoon-Jung Shin, Jae-Won Lee, Yun Chan Kang, Kwang Chul Roh, Pore-tailoring of pruned fruit tree branch derived activated carbon with hierarchical micropore structure for non-aqueous supercapacitors, J. Energy Stor. 56 (2022), 106098.
[64] X. Gong, S.H. Guo, Y.Y. Ding, B. Lou, N. Shi, F.S. Wen, X.J. Yang, G. Li, B. Wu, W. Zhu, D. Liu, Preparation of mesocarbon microbeads as anode material for lithium-ion battery by co-carbonization of FCC decant oil and conductive carbon black, Fuel Process. Technol. 227 (2022) 107,110, https://doi.org/10.1016/j.fuproc.2021.107110.
[65] F. Tuinstra, J.L. Koenig, Raman spectrum of graphite, J. Chem. Phys. 53 (1970) 1126–1130, https://doi.org/10.1063/1.1674108.
[66] Adeela Rehman, Young-Jung Heo, Ghazanfar Nazir, Soo-Jin Park, Solvent-free, one-pot synthesis of nitrogen-tailored alkali-activated microporous carbons with an efficient CO2 adsorption, Carbon 172 (2021) 71–82.
[67] A. Maulana Kurniasari, A.Y. Nugraheni, D.N. Jayanti, S. Mustofa, M.A. Baqiya, Darminto, Defect and magnetic properties of reduced graphene oxide prepared from old coconut shell, in: IOP Conf. Series: Materials Science and Engineering 196, 2017, p. 012021.
[68] J. Serafin, U. Narkiewicz, A.W. Morawski, R.J. Wróbel, B. Michalkiewicz, Highly microporous activated carbons from biomass for CO2 capture and effective micropores at different conditions, J. CO2 Utilizat. 18 (2017) 73–79.
[69] S.W. Choi, J. Tang, V.G. Pol, K.B. Lee, Pollen-derived porous carbon by KOH activation: Effect of physicochemical structure on CO2 adsorption, J. CO2 Utilizat. 29 (2019) 146–155.
[70] M.B. Ahmed, M.A.H. Johir, J.L. Zhou, H.H. Ngo, L.D. Nghiem, C. Richardson, M. R. Bryant, Activated carbon preparation from biomass feedstock: clean production and carbon dioxide adsorption, J. Clean. Prod. 225 (2019) 405–413.
[71] G.K. Parshetti, S. Chowdhury, R. Balasubramanian, Biomass derived low-cost microporous adsorbents for efficient CO2 capture, Fuel 148 (2015) 246–254.
[72] M.G. Plaza, A.S. González, J.J. Pis, F. Rubiera, C. Pevida, Production of microporous biochars by single-step oxidation: Effect of activation conditions on CO2 capture, Appl. Energy 114 (2014) 551–562.
[73] J. Serafin, M. Baca, M. Biegun, E. Mijowska, R.J. Kaleńczuk, J. Sreńscek-Nazzal, B. Michalkiewicz, Direct conversion of biomass to nanoporous activated biocarbons for high CO2 adsorption and supercapacitor applications, Appl. Surf. Sci. 497 (143) (2019) 722.
[74] M. Idrees, V. Rangari, S. Jeelani, Sustainable packaging waste-derived activated carbon for carbon dioxide capture, J. CO2 Utilizat. 26 (2018) 380–387.
[75] J. Serafin, O.F. Cruz Jr., Promising activated carbons derived from common oak leaves and their application in CO2 storage, J. Environ. Chem. Eng. 10 (3) (2022) 107,642.
[76] M. Sevilla, A.B. Fuertes, Sustainable porous carbons with a superior performance for CO2 capture, Energy Environ. Sci. 4 (5) (2011) 1765–1771.
[77] R. Pang, T. Lu, J. Shao, L. Wang, X. Wu, X. Qian, X. Hu, Highly efficient nitrogen-doped porous carbonaceous CO2 adsorbents derived from biomass, Energy Fuel 35 (2) (2020) 1620–1628.
[78] C. Zhang, W. Song, Q. Ma, L. Xie, X. Zhang, H. Guo, Enhancement of CO2 capture on biomass-based carbon from black locust by KOH activation and ammonia modification, Energy Fuel 30 (5) (2016) 4181–4190.
[79] H. Fagnani, C.T. da Silva, M.M. Pereira, A.W. Rinaldi, P.A. Arroyo, M.A. de Barros, CO2 adsorption in hydrochar produced from waste biomass, SN Appl. Sci. 1 (9) (2019) 1–10.
[80] M.G. Plaza, A.S. González, C. Pevida, J.J. Pis, F. Rubiera, Valorisation of spent coffee grounds as CO2 adsorbents for postcombustion capture applications, Appl. Energy 99 (2012) 272–279.
[81] K.K. Kishibayev, J. Serafin, R.R. Tokpayev, T.N. Khavaza, A.A. Atchabarova, D. A. Abduakhytova, J. Sreńscek-Nazzal, Physical and chemical properties of activated carbon synthesized from plant wastes and shungite for CO2 capture. Journal of Environmental, Chem. Eng. 9 (6) (2021) 106,798.
[82] D. Li, Y. Tian, L. Li, J. Li, H. Zhang, Production of highly microporous carbons with large CO 2 uptakes at atmospheric pressure by KOH activation of peanut shell char, J. Porous. Mater. 22 (2015) 1581–1588.
[83] L. Guo, J. Yang, G. Hu, X. Hu, L. Wang, Y. Dong, M. Fan, Role of hydrogen peroxide preoxidizing on CO2 adsorption of nitrogen-doped carbons produced from coconut shell, ACS Sustain. Chem. Eng. 4 (5) (2016) 2806–2813.
[84] Z. Zhao, C. Ma, F. Chen, G. Xu, R. Pang, X. Qian, X. Hu, Water caltrop shell-derived nitrogen-doped porous carbons with high CO2 adsorption capacity, Biomass Bioenergy 145 (105) (2021) 969.
[85] T.A. Khan, E.A. Khan, Removal of basic dyes from aqueous solution by adsorption onto binary iron-manganese oxide coated kaolinite: non-linear isotherm and kinetics modeling, Appl. Clay Sci. 107 (2015) 70–77.
[86] A.L. Myers, J.M. Prausnitz, Thermodynamics of mixed-gas adsorption, AICHE J. 11 (1) (1965) 121–127.
[87] J. Serafin, M. Ouzzine, O.F.C. Junior, J. Sreńscek-Nazzal, Preparation of low-cost activated carbons from amazonian nutshells for CO2 storage, Biomass Bioenergy 144 (105) (2021) 925.
[88] J. Serafin, J. Sreńscek-Nazzal, A. Kamińska, O. Paszkiewicz, B. Michalkiewicz, Management of surgical mask waste to activated carbons for CO2 capture, J. CO2 Utilizat. 59 (2022) 101,970.
[89] J. Serafin, B. Dziejarski, O.F.C. Junior, J. Sreńscek-Nazzal, Design of highly microporous activated carbons based on walnut shell biomass for H2 and CO2 storage, Carbon 201 (2023) 633–647.